The Tyrosyl Free Radical of Recombinant Ribonucleotide Reductase from *Mycobacterium tuberculosis* Is Located in a Rigid Hydrophobic Pocket[†,‡]

Aimin Liu,[§,▽] Stephan Pötsch,[§] Albert Davydov,[§] Anne-Laure Barra,[∥] Harvey Rubin,[⊥] and Astrid Gräslund*[,§]

Department of Biophysics, Arrhenius Laboratories, Stockholm University, S-106 91 Stockholm, Sweden, High Magnetic Field Laboratory, CNRS/MPI, F-38042 Grenoble Cedex, France, and Division of Infectious Diseases, Department of Medicine, University of Pennsylvania School of Medicine, Philadelphia, Pennsylvania 19104

Received June 22, 1998; Revised Manuscript Received August 24, 1998

ABSTRACT: The tyrosyl free radical in protein R2-2 of class Ib ribonucleotide reductase (RNR) from *Mycobacterium tuberculosis* is essential for the enzymatic activity and has an EPR spectrum remarkably similar to that of the tyrosyl radical $Y_D^•$ in PSII. The EPR relaxation properties of the radical suggest a very weak exchange coupling between the two redox centers, the radical and the diferric cluster. The tyrosyl radical gives almost identical EPR spectra in the temperature interval 10−293 K. We conclude that the tyrosyl radical sits in a rigid pocket. Two ring protons and one β-methylene proton account for the major anisotropic hyperfine interactions. A high-frequency EPR spectrum of the radical showed a resolved $g_x = 2.0092$, indicating that a hydrogen bond to the phenolic oxygen of the radical is absent. Theoretical modeling studies based on the structural data known for *Salmonella typhimurium* class Ib RNR protein $R2_F$ revealed a hydrophobic wall aligned with the radical harboring residue Y110. The distance between the phenolic oxygen of the radical and the diferric cluster is longer in the two class Ib *nrdF* R2 proteins than in other characterized class Ia R2 proteins. The tyrosyl radical in protein R2-2 from *M. tuberculosis* was accessible to direct reduction by dithionite in the absence of a mediator. The radical could be partly regenerated when the system was exposed to O_2 after the completion of anaerobic reduction. This indicates that the Fe^{3+} ions also had become reduced by dithionite.

Ribonucleotide reductase catalyses the reduction of ribonucleotides to the corresponding deoxyribonucleotides and therefore plays a central role in DNA biosynthesis and nucleotide metabolism. Several different classes of RNR have been described (*1*−*6*), with a common feature of the radical-based catalytic mechanism (*7*−*8*). All mammalian RNRs, as well as that from aerobically grown *Escherichia coli*, and DNA viruses belong to class I and use nonheme binuclear iron cofactors for generation of the essential tyrosyl radicals. Class I enzymes have been further subdivided into Ia and Ib after the discovery of a new type of *nrdEF* RNR gene and a new pattern of allosteric activity regulation (*9*). The class II RNRs use adenosylcobalamin (coenzyme B_{12}) as a radical generating cofactor (*10*). RNRs isolated from *E. coli* grown under anaerobic conditions (class III) have a glycyl radical that is generated by an iron−sulfur cluster together with *S*-adenosylmethionine (*11*−*13*). An emerging class of manganese-containing RNRs has been proposed and is thought to contain a manganese cluster analogous to the diferric cofactor of class I (*4*, *8*, *14*). However, this remains to be clarified, because RNR from *Corynebacterium ammoniagenes* has recently been found to possess a class Ib amino acid sequence (*15*) and yet is postulated to have an EDTA-inaccessible mononuclear manganese cofactor (*16*).

All class I enzymes are constructed from two homodimeric proteins, R1 and R2 for class Ia RNR and $R1_E$ and $R2_F$ for class Ib RNR (*9*, *17*), coded by the *nrdAB* and *nrdEF* genes, respectively. Substrate and effector binding sites have been localized to $R1/R1_E$. The large protein $R1/R1_E$ is similar in almost all different classes of RNRs.[2] Proteins R2 and $R2_F$ contain the protein-bound tyrosyl free radical that is produced by and stabilized together with a neighboring antiferromagnetically coupled diferric site. RNR in *E. coli* (class Ia) has been extensively investigated since the discovery of the stable tyrosyl radical (*18*). The crystal structure of each of the two components (*5*, *19*−*22*), the generation (*23*, *24*) and the nature of the tyrosyl radical at residue 122 (*25*−*29*), the long-range coupled electron/proton transfer (over 35 Å distance in the two subunits) (*19*−*22*, *30*−*31*), and a substrate−radical catalytic mechanism (*32*) have been postulated or established.

[†] This work was supported by research grants from the Swedish Natural Science Research Council and the Carl Trygger Foundation (A.G.). European TMR program under contract ERBFMGECT950077 is also acknowledged. A.L. acknowledges the Wenner-Gren Center Foundation for a fellowship and the NSFC for a grant (29301004).

[‡] GenBank accession no. U41100 for *M. tuberculosis* R2-2; GenBank accession no. X73226 for *S. typhimurium* $R2_F$.

* To whom correspondence should be addressed. Tel.: +46-8-162450. Fax: +46-8-155597. E-mail: astrid@biophys.su.se.

[§] Stockholm University.

[∥] CNRS/MPI.

[⊥] University of Pennsylvania School of Medicine.

[▽] On leave from the Department of Chemistry, Xiamen University, P. R. China.

[1] Abbreviations: RNR, ribonucleotide reductase (EC 1.17.4.1); PSII, photosystem II; *E. coli*, *Escherichia coli*; *M. tuberculosis*, *Mycobacterium tuberculosis*; *S. typhimurium*, *Salmonella typhimurium*; HSV1, herpes simplex virus type 1; IPTG, isopropyl thiogalactopyranoside; UV−vis, ultraviolet−visible spectroscopy; CD, circular dichroism; EPR, electron paramagnetic resonance; cw-ENDOR, continuous wave electron nuclear double resonance.

[2] Eriksson, M., Kauppi, B., Uhlin, U., Eklund, H. manuscript in preparation.

10.1021/bi981471p CCC: $15.00
Published on Web 10/30/1998

Class Ib ribonucleotide reductases have been recently found in widely different prokaryotes, such as *Salmonella typhimurium*[3], *Lactococcus lactis*, *Mycoplasma genitalium*, and *Mycobacterium tuberculosis*, as well as in anaerobically grown *E. coli* (*9*, *33*−*37*). Class Ib RNRs behave differently from class Ia enzymes in that they are not inhibited by dATP. Instead, dATP stimulates substrate reduction (*34*, *36*). In the cases known, class Ib RNRs are normally not expressed in vivo under normal laboratory growth conditions, with the only exception so far being *M. tuberculosis* RNR. From a previous study of *S. typhimurium* $R2_F$ (*38*) and the results presented in this study, it seems that the EPR spectra of the tyrosyl free radical of class Ib RNRs are distinct from those of R2s of class Ia enzymes. Instead, they are strikingly similar to those of the tyrosyl radicals $Y_D^•$ and $Y_Z^•$ from wild-type and mutant PSII (*38*−*44*).

Class Ib RNR from the Erdman strain of *M. tuberculosis* was recently isolated, sequenced, and expressed in *E. coli* (*45*, *46*). *M. tuberculosis* RNR is allosterically regulated with ATP or dATP as activators for CDP reduction up to 2 and 1 mM, respectively. The native enzyme consists of two nonidentical components, i.e., proteins $R1_E$ and $R2_F$, both required for activity. The large subunit $R1_E$ of *M. tuberculosis* RNR has a predicted molecular mass of 2 × 82.244 kDa (*46*). The *M. tuberculosis* genome (*47*) contains two genes, *nrdF1* and *nrdF2*, that encode small RNR components denoted R2-1 and R2-2, respectively. Both are postulated to contain an iron−radical site like other class I R2 proteins (*46*). The recombinant R2-2 is enzymatically active when assayed with recombinant protein $R1_E$ in the presence of ATP/dATP and substrate CDP. R2-2 has 21−23% sequence identity to the *E. coli nrdB* gene product and 16% identity to the human R2 protein. It is a dimer and has a calculated molecular mass of 2 × 36.957 kDa (the monomer contains 324 amino acids). Alignment analysis established that all essential conserved amino acids corresponding to the *E. coli* radical-harboring residue 122, the iron-binding residues, and the residues forming the hydrophobic pocket around the stable radical are conserved in the *M. tuberculosis* R2-2 protein. Site-directed mutagenesis of Y110 to phenylalanine has demonstrated that the free radical is located at the tyrosyl residue 110. Protein R2-2 can be inactivated by hydroxyurea, which acts as a radical scavenger and destroys the tyrosyl radical (*46*).

The RNR enzyme from the pathogen *M. tuberculosis* has attracted attention, because tuberculosis remains a major global disease infecting one-third of the world population and killing 3 million people each year. Its complete genome sequence was recently reported (*47*). *M. tuberculosis* has been described as the only bacterial species identified so far in which the *nrdEF* system appears to encode the biologically active form of class Ib RNR components (*9*, *45*, *46*). Thus far, seven sequences (including at least two completed sequences) for protein $R2_F$ in class Ib enzymes have been reported (*3*, *33*−*37*, *46*−*48*). In this study, we present the first comprehensive characterization of the tyrosyl radical in the class Ib protein R2 from *M. tuberculosis*.

[3] The X-ray crystal structure of protein $R2_F$ from *S. typhimurium* has recently been resolved at 2.0 Å resolution. Eriksson, M., Jordan, A., and Eklund, H. (1998) *Biochemistry 37*, 13359−13369, Brookhaven Data Bank entries 1r2f and 2r2f.

EXPERIMENTAL PROCEDURES

Expression and Fermentation of $R2_F$ from M. tuberculosis RNR. A colony of bacteria containing the gene for R2-2 inserted into a pET-11a vector was grown overnight to 0.6 OD at 30 °C in 10 mL of Luria broth supplemented with ampicillin (100 μg/mL). The next day, 200 mL of the same medium was inoculated with 0.8 mL of cultures grown overnight. Finally, 6 L of the same medium was inoculated with the 200 mL cultures (0.6−0.8 OD) to 0.002 OD at 640 nm and shaken vigorously (250 rpm) at 30 °C. At $A_{640} = 0.8$, IPTG was added to a final concentration of 0.5 mM to induce overproduction of the cloned R2 gene. Growth was continued until late log stationary phase at $A_{640} = 2.1-2.3$ (typically after 2.5 h of induction). The cells were quickly chilled on ice and harvested by centrifugation. Pellets were frozen on dry ice and stored at −80 °C. Cells were grown on iron-depleted amino acid minimum medium as described elsewhere (*49*).

Protein Purification. Frozen cells of recombinant *E. coli* paste were disintegrated through an X-press (BIOX) and resuspended in extraction buffer containing 50 mM Tris−HCl, pH 7.6, 20% glycerol, 0.02 mM dithiothreitol, and 0.05 mM phenylmethylsulfonyl fluoride. Unless otherwise indicated, all purification procedures were carried out at 4 °C. The protocol used was as previously described (*46*), with the slight modification that we replaced the long dialysis step with a G-25 desalting column just before the DE−52 (Whatman) anion-exchange chromatography. HPLC (Superose 12 HR, 10/30, with flow rate of 0.4 mL/min and 10 bar on LC-10AD, Shimadzu) and Phast-Gel (Pharmacia) analysis indicated that the purity was more than 95% and suitable for most characterization purposes. The final purification step used for the sample investigated by CD spectroscopy was FPLC ion-exchange chromatography on a Mono-Q 10/10 column from Pharmacia with 50 mM Tris−HCl, pH 7.6, 0.02 mM DTT. The recombinant *M. tuberculosis* R2-2 was dialyzed with HEPES buffer (pH 7.6) in an Amicon concentrator. The protein concentration was determined by Bradford assay. *E. coli* R2 was purified as described previously (*50*).

Protein Reactivation. Purified native R2-2 protein in O_2-saturated buffer and argon-saturated $(NH_4)_2Fe(SO_4)_2·6H_2O$ solution (giving a $4Fe^{2+}$/R2-2 ratio) were mixed in equal volumes at room temperature. The reaction was performed in 50 mM Tris−HCl or HEPES buffer, pH 7.6. A subsequent desalting step to remove unspecifically bounded iron was carried out on a 1 cm × 6 cm Sephadex G-25 column.

Chemical Reduction. Anaerobic reduction was performed by the addition of microliter volumes of argon-saturated stock solution of dithionite to R2-2 protein in 50 mM Tris−HCl, 100 mM KCl, pH 7.6 buffer prepared by gently flushing with argon for 60 min on ice. The reaction was followed on a Varian Cary-4 UV−vis spectrometer at 15 °C.

Light Absorption and Protein Concentration. The active *M. tuberculosis* $R2_F$ protein was analyzed by UV−vis spectroscopy using either a Varian Cary-4 (equipped with a temperature controller) or a Perkin-Elmer 200 spectrophotometer.

Circular Dichroism (CD) Spectroscopy. CD measurements were carried out using a JASCO J-720 spectropolarimeter with 1.0 mm light path cuvettes at 4 °C. The

parameters used were a bandwidth of 1 nm, a resolution of 0.2 nm, and a scan speed of 100 nm/min.

X-Band EPR Measurements. EPR spectra at 9.45 GHz between 5 and 293 K were recorded on a Bruker ESP 300 spectrometer. A coldfinger Dewar flask with liquid nitrogen was used for 77 K measurements. The 100 and 200 K measurements were accomplished by a liquid nitrogen continuous-flow system with a temperature controller. A 250 μL flat-cell from Wilmad (0.7 mm thickness) was used for the room-temperature EPR studies. All temperatures below 77 K were achieved by using an Oxford Instruments continuous-flow liquid helium cryostat. Quantitation of the EPR signals was performed by double integration of the spectra recorded under nonsaturating conditions and comparison with a standard sample of wild-type R2 from *E. coli* in which the radical content was previously calibrated with a sample of 1 mM $CuCl_2$, 10 mM EDTA (pH 7.5 at 20 °C). A Bruker 035M NMR gaussmeter was used for *g*-value determination.

High-Field EPR Studies. EPR spectra of purified *M. tuberculosis* R2-2 and *E. coli* R2 at 285 GHz were recorded at 5 K with a maximum 3 G modulation amplitude in the High Magnetic Field Laboratory (CNRS/MPI, Grenoble, France). The frequency source used to generate a 285 GHz excitation is a Gunn diode delivering a 95 GHz basic frequency, which is then tripled to obtain 285 GHz (system supplied by Radiometer Physics GmbH). The basic frequency can be changed by $\pm$50 MHz. The exact frequency used was recorded automatically by the system. The high-field EPR system has been previously described (*51*).

Simulation of EPR Spectra. EPR spectra at 9.45 and 285 GHz were simulated by the following strategy: the *g*-tensors determined directly from the high-frequency spectrum were used for the X-band iteration minimization routines to fit the spectrum, and then the hyperfine couplings determined from X-band simulation were used for the high-frequency spectrum simulation. Spectra simulations were performed by using an iterative fitting program (52) as previously described (*38*, *53*).

Building the Structural Model of M. tuberculosis R2-2. The coordinates of *S. typhimurium* $R2_F$ were generously provided by Prof. H. Eklund in PDB format[3] and used as the starting point for the model building of the *M. tuberculosis* R2-2. The amino acid substitutions (point mutations) based on the sequence data of the two proteins were produced by Insight II (a molecular modeling program from BIOSYM Technologies) on a Silicon Graphics Workstation. Energy minimization was performed on a Pentium Pro personal computer by the program MM2,[4] which is built in the molecular modeling program Chem3D (ChemOffice Ultra98, CambridgeSoft).

RESULTS

The Secondary Structures of M. tuberculosis R2-2. The highly purified *M. tuberculosis nrdF* protein R2-2 was golden in color when concentrated and harbors a tyrosyl free radical which was unchanged after storage at room temperature for at least 8 h, as monitored by EPR and optical spectroscopy. The CD spectrum of protein R2-2 is given as Supporting Information (Figure 1s). It is almost identical to that of *E. coli nrdB* R2 protein in contrast to the low identity (21−23%) of amino acids in their peptide sequences. The CD spectra are in agreement with an α-helix-dominated secondary structure in both proteins as shown in the crystal structure of *E. coli* R2 (*19*−*21*).

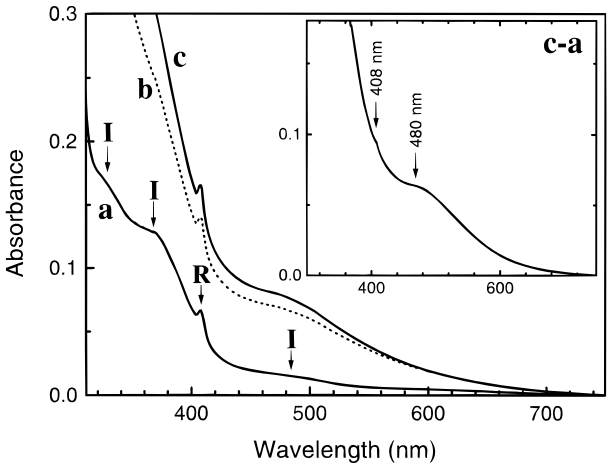

FIGURE 1: Light absorbance spectra of protein R2-2 from *M. tuberculosis*: (a) in 50 mM Tris−HCl, pH 7.6, 0.1 M KCl; with additional exogenous ferrous ions ($4Fe^{2+}$/R2), after 2 min (b) and 30 min (c) incubations.

The Radical and Iron Content. The free radical content in the freshly prepared *M. tuberculosis* protein R2-2 corresponds to 0.3−0.4 radical/R2-2 as quantified by X-band EPR. The iron content was found to be less than the expected four times the stoichiometric amount. Exogenous addition of ferrous ions to purified protein R2-2 resulted in approximately 2.5 times higher EPR signal intensity of the free radical, indicating a substantial loss of the radical and iron ions during the purification. This suggests that the iron center in R2-2 is more labile compared to that of *E. coli* R2. In contrast, protein R2 of recombinant mouse RNR was in an essentially iron-free form after column preparation and has the lowest stability of the iron centers among the class I RNRs investigated by us. The reconstitution reaction of apoR2-2 (metal-free) with Mn^{2+}, Ni^{2+}, Co^{2+}, Zn^{2+}, Cd^{2+}, and Mg^{2+} in the presence of molecular oxygen did not produce the tyrosyl radical as does reaction with Fe^{2+}.

Concentrations of *M. tuberculosis* protein R2-2 were determined spectrophotometrically by using molar absorption coefficients at 280 and 310 nm. The extinction coefficient $\epsilon_{280-310}$ for R2-2 was measured to be 118 000 M^{-1} cm^{-1} on the basis of a Bradford protein concentration assay.

Electronic Spectra of Protein R2-2. Active *M. tuberculosis* protein R2-2 exhibits a highly characteristic electronic spectrum between 320 and 650 nm, with a tyrosyl radical peak at 408 nm (ϵ_{408} = 5578 M^{-1} cm^{-1}). The dominant features of the diferric cluster in R2-2 are absorption bands at 325 and 370 nm, as well as a broad feature in the 480 nm area and a very weak band at 620 nm (Figures 1 and 2). These iron-related peaks or shoulders are well-known and are also observed in *E. coli* R2 and hemerythrin (*54*). Both the radical- and iron-related absorbances increased consider-

[4] The best source of information on the MM2 parameter set is Burkert, U., and Allinger, N. L. (1982) *Molecular Mechanics*, ACS Monograph 177, American Chemical Society, Washington, DC. A method for parameters for non-MM2 atom types can be found in Development of an Internal Searching Algorithm for Parametrization of the MM2/MM3 Force Fields (1991), *J. Comput. Chem. 12*, 844−849.

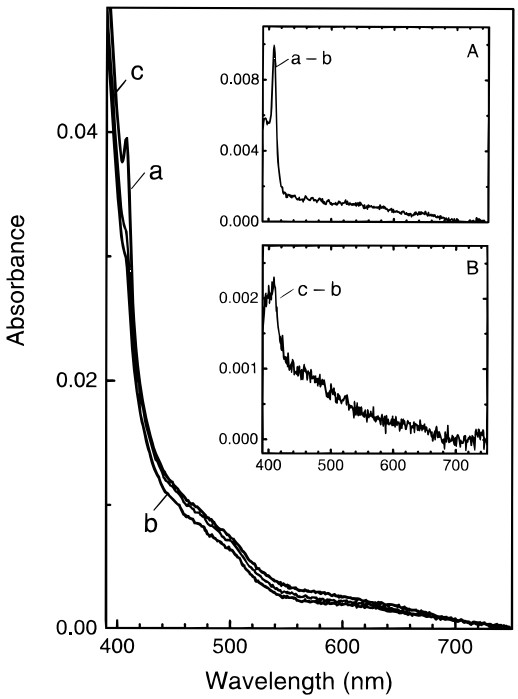

FIGURE 2: Light absorbance spectra of *M. tuberculosis* R2-2 protein in the presence of dithionite: (a) initial state, protein (45 uM) and dithionite (250 uM); (b) after 114 min anaerobic reduction; (c) after admission of air to b. The insets are the differences among a, b, and c: (A) the difference (a − b) displays the reduction of the tyrosyl radical; (B) the difference (c − b) shows partially regenerated tyrosyl radical after the admission of air.

ably (Figure 1) when the protein was reactivated with $(NH_4)_2$-$Fe(SO_4)_2 \cdot 6H_2O$ in the presence of molecular oxygen. The 370 nm absorption has been characterized as an oxo → iron charge transfer band, which should originate from the O^{2-} bridge between the two antiferromagnetically coupled ferric irons. The golden color of highly concentrated R2-2 protein remained unchanged when the protein was treated by the radical scavenger hydroxyurea. The color of active protein R2-2 was much deeper than that of the iron-free protein purified from cells grown in iron-depleted medium. Therefore, the golden color and the other iron-related bands are most likely due to a ligand → iron charge transfer, similar to the situation in purple acid phosphatase (*55*).

Chemical Reduction of the Redox Centers. The single oxidation equivalent located at the tyrosyl residue Y110 in protein R2-2 could be reduced anaerobically with excess dithionite in the absence of a mediator. Figure 2 shows 45 μM protein R2-2 under reaction with 250 μM sodium dithionite. The reaction is essentially completed after ca. 3−4 h incubation at room temperature. Inset A of Figure 2, which is the difference between the initial state and after 114 min of reduction, shows that the optical absorption bands of the radical and iron were clearly changed by reduction. The kinetics is biphasic. Under the same reaction conditions (i.e., dithionite in less than 10 times excess), protein R2 from *E. coli* did not show dithionite sensitivity in the absence of mediators on a time scale of 4 h. A clearly detectable increase of the free radical content in protein R2-2 appeared when the system was exposed to air after the completion of the dithionite reduction. The resulting spectrum is shown in spectrum c of Figure 2, and the difference is given in inset B. We conclude that part of the diiron clusters had also been reduced in the previous reduction, because the radical regeneration reaction requires participation of ferrous iron ions. The iron center was being reduced much more slowly than the tyrosyl radical.

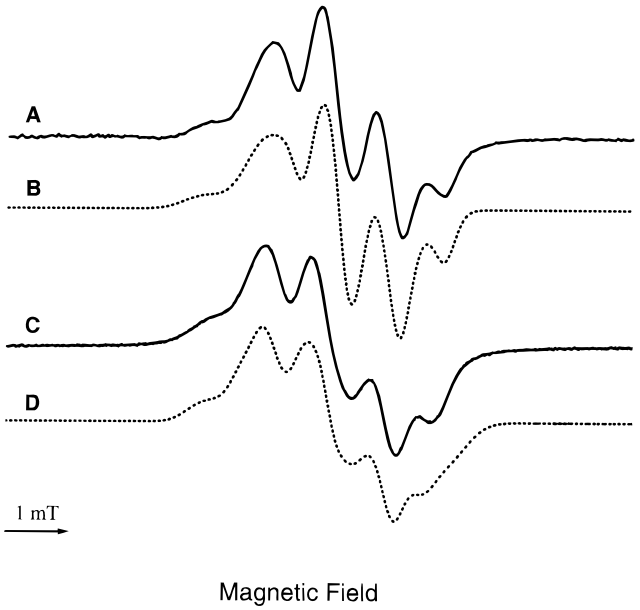

FIGURE 3: X-band EPR spectra of protein R2-2 (A) in frozen solution (10 K) and (C) in liquid solution (293 K). All spectra were obtained under nonsaturated conditions. Solid lines: experiment; dotted lines: best simulation fit. The 10 K spectral parameters are shown in Table 1. The parameters used for the simulation of the spectrum at 293 K were similar (not shown).

Table 1: Anisotropic Hyperfine Couplings[a] of Tyrosyl Radicals in *M. tuberculosis* R2-2 Protein and *S. typhimurium* $R2_F$ from Simulations of EPR Spectra Measured at 10 K[b]

	S. typhimurium $R2_F$ (ref 38)			*M. tuberculosis* R2-2 (this work)		
	A_x	A_y	A_z	A_x	A_y	A_z
$H_{\beta 1}$	10.5	7.4	9.5	8.9	7.3	9.0
$H_{3,5}$ (ring)[c]	−11.5	−2.5	−7.1	−11.7	−1.9	−7.1
$H_{2,6}$ (ring)[d]	<3.0	<3.0		2.8	2.0	1.1

	S. typhimurium $R2_F$ (ref 38)			*M. tuberculosis* R2-2 (this work)		
	LW_x	LW_y	LW_z	LW_x	LW_y	LW_z
line width (G)	5.8	5.3	3.7	5.80	5.4	2.9

[a] Hyperfine couplings are given in gauss. [b] The coordinate system is such that the *z*-axis is perpendicular to the plane of the tyrosyl ring and the *x*-axis is along the C4−O4 direction. For numbering see Figure 6B. [c] Average value of 3 and 5 protons. The direction of the eigenvector corresponding to the smallest eigen-value had an angle about 70° from the *x* direction, to be compared with the theoretically expected 60°. [d] From preliminary cw-ENDOR spectra of *M. tuberculosis* R2-2.

EPR Hyperfine Structure and Relaxation Properties of the Tyrosyl Radical. The recorded X-band EPR spectrum of active *nrdF* R2-2 is dominated by the tyrosyl radical signal with an approximate average *g*-value determined from the baseline crossing of a 10 K spectrum as $g = 2.0053$ ($\pm 3 \times 10^{-4}$). Figure 3 shows the X-band EPR spectra at 10 and 293 K, together with simulated spectra in dotted traces. The hyperfine parameters are presented in Table 1. It is remarkable that the tyrosyl radical of *M. tuberculosis* R2-2 gave almost identical EPR spectra in this wide temperature

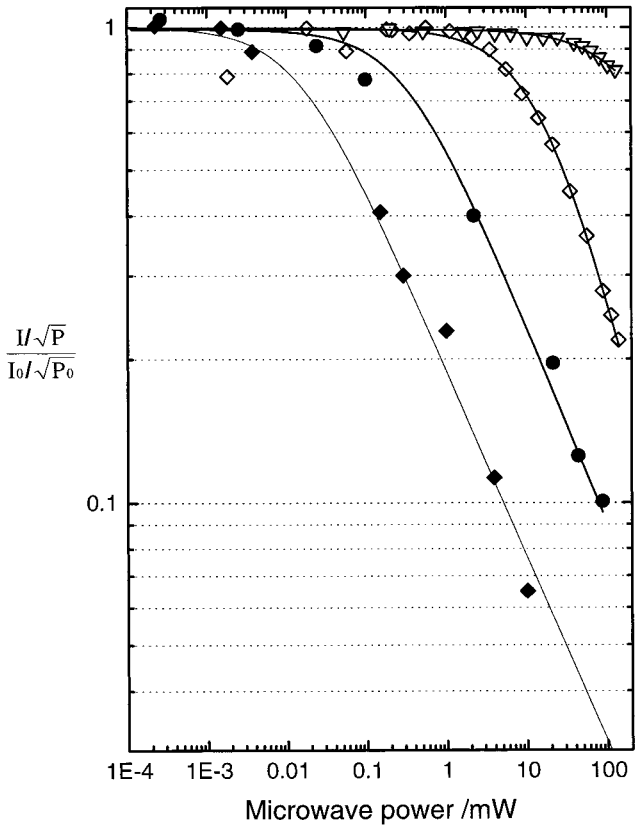

FIGURE 4: Representative EPR microwave power saturation curves of the tyrosyl radical in the temperature range 5−293 K. Continuous traces are computer fits as described in the text. (◆) 5 K, (●) 30 K, (□) 200 K, (▽) 293 K.

range. The binuclear iron cluster is EPR-silent due to the antiferromagnetic coupling of the two high-spin ferric ions. As in the case of *E. coli* R2, a minor signal at $g = 4.3$ was also observed at low temperatures and attributed to nonspecifically bound Fe^{3+} in a rhombic symmetry, corresponding to less than 2% of the total iron in active R2-2 (not shown). The X-band EPR spectrum of R2-2 is virtually identical to the spectrum of *S. typhimurium* $R2_F$ (*38*) and remarkably similar to the radical $Y_D^\bullet$ of PSII (*39*−*44*). One β-methylene proton and the 3,5 ring protons (for numbering see Figure 6B) give significant hyperfine couplings in the EPR spectra (Table 1). The contribution of the second β-methylene proton is hidden in the EPR line width. The hyperfine coupling parameters were verified by preliminary cw-ENDOR spectra (not shown), which also resolved anisotropic signals from weakly coupled protons that we assign here to the 2,6 ring protons (Table 1).

The EPR relaxation behavior of protein R2-2 at different temperatures is presented in Figure 4. The microwave saturation occurs at very low microwave power at each measured frozen temperature. Table 2 gives the parameters of the saturation curves in terms of the microwave power at half saturation $P_{1/2}$ and b, which describes the contribution of inhomogeneous broadening (*56*):

$$I \propto 1/(1 + P/P_{1/2})^{b/2} \quad (1)$$

where I is EPR amplitude and P is microwave power. The presence of inhomogeneous broadening as judged from b values close to 1 can be inferred from Table 2. The most

Table 2: EPR Relaxation Parameters of the Tyrosyl Radical in R2-2 Protein from *M. tuberculosis*[a]

	temp (K)									
	5	10	20	30	40	50	77	100	200	293[b]
$P_{1/2}$ (mW)	0.01	0.09	0.25	0.31	0.37	0.62	0.72	1.28	15.60	144.23
b	0.78	0.71	0.88	0.82	0.76	0.65	1.25	1.23	1.37	0.67

[a] $P_{1/2}$ and b values were estimated from computer fitting of microwave saturation curves. [b] The saturation with 140 mW microwave power at 293 K is only about 20%. The $P_{1/2}$ and b values for this temperature were approximately estimated from computer fitting.

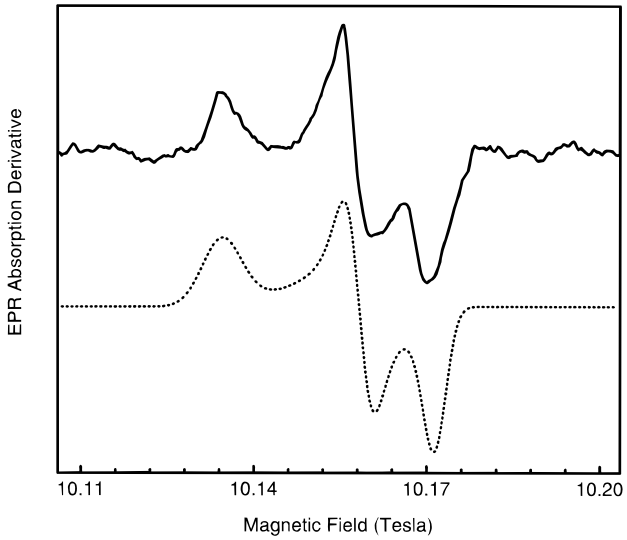

FIGURE 5: 285 GHz high-field EPR spectrum of *M. tuberculosis* R2-2 at 5 K. Measurement conditions: field modulation 15.06 mA, time constant 300 ms, sweep time 890 s. Solid line: experiment; dotted line: simulation.

straightforward interpretation for the easily saturated radical spectra with small $P_{1/2}$ values is that the tyrosyl radical is minimally influenced in its relaxation by the diferric cluster. The EPR anisotropic pattern of the R2-2 tyrosyl radical observed in liquid solution at room temperature is almost the same as that observed at 10 K (Figure 3). The results also indicate that at room temperature there is little influence on the radical relaxation by the iron site (Figure 4).

High-Field EPR Characterization of the Tyrosyl Radical in M. tuberculosis R2-2. High-field EPR at 285 GHz using a magnetic field of 10.1 T was applied to probe the chemical environment and g-value anisotropy of the radical. The three g-value components are clearly resolved (Figure 5). The total g-anisotropy was found to be 0.0070. The average g-value was determined from X-band EPR to be approximately 2.0053 ($\pm 3 \times 10^{-4}$), which leads to the three components 2.0092, 2.0046, and 2.0022 for g_x, g_y, and g_z, respectively (Table 3). These values were used as starting parameters for the simulation of the X-band spectrum (Figure 3B,D) and were found to be unchanged in the iterative procedure. The high-field EPR spectrum was simulated directly using the parameters of the X-band simulation without iterations. The fit was found to be quite satisfactory (Figure 5). The error margins of the g-tensor components are the same as for the average g-value ($\pm 3 \times 10^{-4}$) due to uncertainties in field and frequency determinations. The g-tensor components of the tyrosyl radical in protein R2-2 are very similar to those determined for the *E. coli* and *S. typhimurium* tyrosyl

Table 3: EPR *g*-Tensor Components for Tyrosyl Radicals in *E. coli* R2, Mouse R2, Photosystem II $Y_D^\bullet$, *S. typhimurium* $R2_F$, and *M. tuberculosis* R2-2 Protein

	g_x	g_y	g_z	ref
E. coli R2	2.0087	2.0042	2.0020	41
	2.0091	2.0046	2.0023	27
Mouse R2	2.0076	2.0043	2.0022	53
PSII $Y_D^\bullet$	2.0075	2.0042	2.0021	41
S. typhimurium $R2_F$	2.0089	2.0043	2.0021	38
M. tuberculosis R2-2	2.0092	2.0046	2.0022	this work

radicals (*26*−*28*, *38*). The g_x of 2.0092 is typical for the non-hydrogen-bonded phenolic oxygen of the neutral tyrosyl radical, thus distinguished from the hydrogen-bonded tyrosyl radical of, for example, $Y_D^\bullet$ (2.0075) (*41*). The g_z value of 2.0022 is close to that of a free electron, as expected.

A Theoretical Structure Model of M. tuberculosis R2-2 and the Tyr110 Environment. A three-dimensional molecular model (Figure 6A) for *M. tuberculosis nrdF* protein R2-2 was built by adapting the crystal coordinates of *S. typhimurium nrdF* $R2_F$ that were determined in an X-ray crystallographic study.[3] The overall structure of protein R2-2 should be very similar to that of *S. typhimurium* $R2_F$. The EPR spectra of the tyrosyl radical in the two proteins are almost identical. The two proteins belong to the same class Ib RNRs and have 77% sequence identity. All iron ligands and mechanism-related residues (especially those involved in forming the hydrophobic pocket for the radical and in the electron/proton transfer pathway) are conserved in both proteins. In particular, the residues shown in Figure 6A are all identical in the two proteins. We reasoned that it should be meaningful to construct a point-mutation variant starting from the 2.0 Å crystal structure of *S. typhimurium* $R2_F$. Energy minimization was performed on the model using the program MM2 as described in the Experimental Procedures.

The overall features of the model of *M. tuberculosis* R2-2 are similar to those of the crystal structure of *S. typhimurium* $R2_F$. In particular, the iron−radical sites (Figure 6A) agree very well. However, small differences in the iron−ligand arrangement were observed: Glu197 is a bridging ligand in *M. tuberculosis* R2-2, whereas it ligates only Fe_2 in *S. typhimurium* $R2_F$, and Glu163 is a bidentate ligand to Fe_2 in *M. tuberculosis* R2-2, whereas it is monodentate in *S. typhimurium* $R2_F$ (Figure 6B). There remain some uncer-

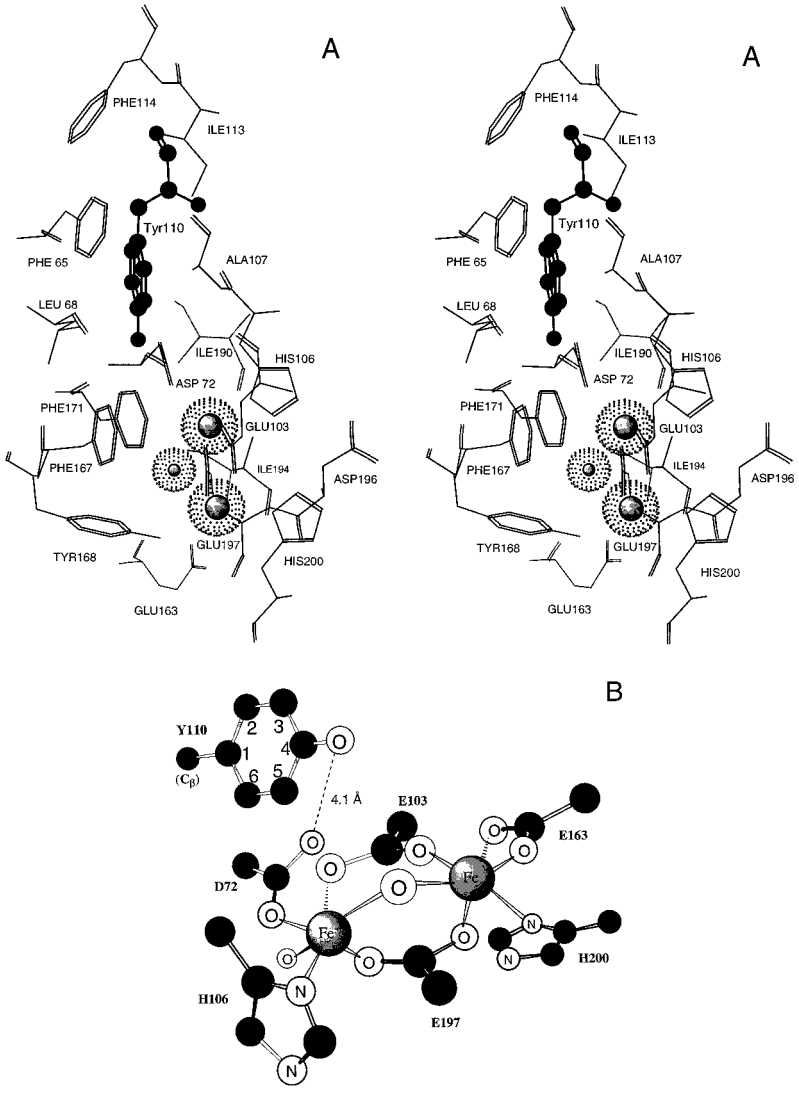

FIGURE 6: Surrounding of the tyrosyl free radical in stereoview (panel A) and the model of the diferric center (panel B) in *M. tuberculosis* protein R2-2 deduced from a molecular modeling study based on the crystal coordinates from *S. typhimurium* $R2_F$.[3] The radical harboring tyrosine 110 and the μ-oxo bridged iron ions are shown by ball-and-stick mode, and others are in wire-frame mode (in panel A).

tainties about the number and well-defined locations of water molecules in the structures.

The coordination details in this model of the iron site and the adjacent radical in R2-2 are shown in Figure 6. Asp72, Glu103, His106, Glu163, Glu197, and His200 are iron ligands, corresponding to Asp84, Glu115, His118, Glu204, Glu238, and His241 in *E. coli* R2, respectively. The two iron ions are bridged by two carboxylates of Glu103 and Glu197 and a μ-oxo bridge, in excellent agreement with the electronic spectra of R2-2 (Figure 1). The most striking difference between this diiron site and that of *E. coli* R2 is Asp72. It ligates Fe_1 in a monodentate fashion in R2-2 and is not in a hydrogen-bond distance from the phenolic oxygen of the tyrosine residue (Figure 6B). The distance between the phenolic oxygen of the radical and the closest iron ion is long, 6.7 Å, in contrast to 5.3 Å in *E. coli* R2, and the backbone of Asp72 is located midway between the tyrosyl radical and the diiron site. This provides a possible explanation to the weak influence of the iron site on the EPR relaxation properties of the tyrosyl radical.

The highly conserved Phe167 and 171 (208 and 212 for *E. coli* R2 numbering) produce a big clip to hold the diiron center (in particular, Fe_1) and more or less fix the position of the Fe_1 ion. The hydrophobic pocket surrounding the radical is further composed by Phe65, Ile113, Phe114, and Ile190. The tyrosyl ring is sandwiched between Phe65 and Ile190, whereas Ile113 and Phe114 are close to the β-methylene position. Leu68, Phe167, and Phe171 are located in front of the phenolic oxygen of the radical. All of these amino acids are highly conserved in class Ib RNR enzymes, implying a common environment for the tyrosyl radicals in this subclass.

DISCUSSION

Class Ia and Ib RNRs are differentiated by substantial sequence differences. However, class Ib RNRs seem to have a high structural homology with class Ia enzymes, judging from CD spectroscopy on *M. tuberculosis* RNR R2-2 (Figure 1s, Supporting Information) and the recently determined three-dimensional structure of *S. typhimurium* $R2_F$ protein[3] as compared to the corresponding data for *E. coli* R2 (19−21). Also, the light absorption spectra (Figure 1) monitoring the iron site and the free radical on Y110 in *M. tuberculosis* R2-2 seem to be quite similar to the other members in the class I RNRs.

The reduction by dithionite of the iron−free radical site is slow but significant in *M. tuberculosis* R2-2 (Figure 2), in contrast to *E. coli* R2 but similar to the situation in mouse R2. The difference between *E. coli* R2 and mouse R2 in this respect has been attributed to a more open structure in mouse R2, making the iron−free radical site more accessible to external reductant than in *E. coli* R2 (*22*, *57*). Hence, we expect a relatively open site in *M. tuberculosis* R2-2 also. The ease of reduction of the iron ions may be important for the enzyme activity, because the tyrosyl radical, if lost, can only be regenerated in a reaction between a reduced iron site and molecular oxygen.

The hyperfine structure of the tyrosyl free radical seems to be a distinguishing spectral feature between class Ia and Ib R2 proteins. Both *S. typhimurium* $R2_F$ (*38*) and *M. tuberculosis* R2-2 proteins give EPR spectra which are much narrower than those in class Ia proteins (Figure 3). The hyperfine couplings $A_{\beta1}$ and $A_{\beta2}$ of the methylene protons are related to the dihedral angles β as follows (*58*, *59*):

$$A_{\beta1} = \rho(B_o + B_1 \cos^2 \beta) \quad (2)$$

$$A_{\beta2} = \rho(B_o + B_1 \cos^2 (\beta + 120°)) \quad (3)$$

A theoretical study has indicated that a tyrosyl radical has two energy minima when the dihedral angles β of the methylene protons are varied (*60*). A local energy minimum corresponds to the β dihedral angles in class Ia enzymes, whereas the global minimum corresponds to the β dihedral angles of the tyrosyl radical in *S. typhimurium*, *M. tuberculosis*, and PSII proteins. The average value of the larger $H_{\beta1}$ hyperfine coupling in *M. tuberculosis* R2-2 is 8.4 G (Table 1). Using eqs 2 and 3 and the same parameter values as in ref 28, we obtained the dihedral angles for the two β methylene protons (Table 4). These β dihedral angles are strikingly identical in *M. tuberculosis* R2-2 and the recently reported PSII $Y_D^\bullet$ radicals (*44*). However, in the present case, the geometry is not completely determined because the two angles may be interchanged. The hyperfine couplings of the 3,5 ring protons are essentially the same as in class Ia tyrosyl radicals ($A_{3,5} = -9.5$, -3.0, and -7.0 G in *E. coli* R2) (28) and agree with the previous conclusion that the spin densities of the neutral tyrosyl radicals are almost invariant (*25*−*29*, *38*, *43*, *60*).

Table 4: Dihedral Angles of the β-Methylene Protons of Tyrosyl Radicals in RNR and PSII

tyr$^\bullet$	θ_1 (deg)[a]	θ_2 (deg)	ref
M. tuberculosis R2-2	52 ± 6	68 ± 6	this work
E. coli R2	30 ± 3	90 ± 3	26
PSII ($Y_D^\bullet$)	52 ± 4	68 ± 4	44

[a] θ_1 and θ_2 represent the dihedral angles between the $2p_z$ orbital at C1 and the planes containing the C1−Cβ−Hβ_1 bonds and the C1−Cβ−Hβ_2 bonds, respectively.

It should be emphasized that the almost identical EPR spectra observed for *M. tuberculosis* R2-2 at 10 K and room temperature (Figure 3A,C) show that at all temperatures the tyrosine 110 ring is in the same locked conformation, which is reflected in the invariant dihedral angles of the β-methylene protons over the whole temperature range. This means that the tyrosyl radical sits in a steric rigid environment, which is also supported by the molecular modeling studies. This finding of a well-resolved EPR signal of the tyrosyl radical in protein R2-2 at room temperature may facilitate the monitoring of the catalytic reaction in situ in the future mechanism studies.

A second distinguishing EPR characteristic reflecting the geometry of the tyrosyl radicals in different R2 proteins is the magnetic interaction with the nearest iron ion in the diiron site. The three-dimensional structure of *S. typhimurium* $R2_F$ protein showed a distance of 6.5−7.0 Å between the iron and the hydroxyl oxygen of tyrosine,[4] compared to about 5.2−5.3 Å in *E. coli* R2 (*19*−*21*). The modeled structure of *M. tuberculosis* R2-2 also appears to have a long iron−radical distance (6.7 Å), and this is consistent with its EPR microwave saturation behavior (Figure 4). Almost no magnetic interaction between the iron ions and the radical is seen, not even at room temperature, where the magnetic moment of the iron site should be significantly high. By

contrast, for *E. coli* R2 or to an even more extreme degree for mouse R2, room-temperature tyrosyl radical EPR spectra are severely broadened due to magnetic interaction between the radical and the rather high magnetic moment of the nearby iron site (*7*). The results suggest that a large distance between the iron site and radical and possibly a different angular arrangement compared with *E. coli* R2 is a characteristic of the *M. tuberculosis* R2-2 protein.

The principal values of the *g*-tensor of the radical are directly observed in the high-field EPR spectrum. Here we found that the highest *g*-tensor component, g_x, is 2.0092, closely similar to that of *E. coli* R2. The magnitude of the g_x component is an indicator of the absence or existence of an H-bond to the radical phenoxy group (*27*, *41*, *42*). A high g_x value as seen here indicates the absence of such an H-bond. Because it is believed that the H bonding partner in the cases where it has been found, e.g., in mouse R2 (*53*), is a water ligand to the closest iron ion (*29*), it makes sense that it is absent in *M. tuberculosis* R2-2 with its presumed long distance between the iron ions and the radical.

The absence of an H-bond to the tyrosyl radical in the prokaryotic R2 proteins characterized in this respect (*E. coli*, *S. typhimurium*, and *M. tuberculosis*) in contrast to the situation in mouse or HSV1 R2 is somewhat surprising. It should also be pointed out that the PSII tyrosyl radical $Y_D^{\bullet}$, despite the similar geometry of the β-methylene protons, is different in this respect and is clearly H-bonded (*39*−*44*). One would expect that the H-bond is crucial for the function of the R2 radical during the catalytic reaction, when its radical property is proposed to be transferred along the H-bonded radical transfer chain to a substrate binding site in protein R1 (*5*−*8*, *19*−*22*, *30*, *31*). A speculative explanation is that the enzymatic activity requires a conformational change in protein R2, brought about by interaction with protein R1 loaded with substrate and allosteric effectors, and that this change leads to the formation of a connecting H-bond to the radical.

In summary, the tyrosyl radicals in class Ib RNRs seem to have a common geometry different from those in class Ia enzymes. This is reflected both in the β-methylene dihedral angles and in the long distance to (and weak interaction with) the iron site. That the rigid environment around the radical does not allow rotation of the tyrosyl ring at room temperature has been established for the first time in the protein R2-2 from *M. tuberculosis*. This may be of functional importance for enzymatic reactions in class I ribonucleotide reductases.

ACKNOWLEDGMENT

We thank Prof. A. Ehrenberg for constructive suggestions and discussions, Prof. W. Lubitz, Technical University Berlin, for the opportunity to work in his laboratory for the cw-ENDOR measurements, and Prof. H. Eklund for making available the coordinates of the *S. typhimurium* $R2_F$ protein prior to publication. Dr. P. Allard is acknowledged for his assistance in EPR spectra simulations. We are indebted to Mr. T. Astlind for excellent technical support in all the spectroscopic measurements.

SUPPORTING INFORMATION AVAILABLE

One figure (Figure 1s) of the CD spectra of highly purified recombinant *M. tuberculosis* R2-2 and wild-type *E. coli* R2 (1 page). Ordering information is given on any current masthead page.

REFERENCES

1. Reichard, P. (1993) *Science 260*, 1773−1777.
2. Stubbe, J. (1990) *Adv. Enzymol. Relat. Areas Mol. Biol. 63*, 349−419.
3. Sjöberg, B. M. (1995) in *Nucleic Acids and Molecular Biology* (Eckstein, F., and Lilley, D. M. J., Eds.) pp 192−121, Springer-Verlag, Berlin, Heidelberg.
4. Stubbe, J., and van der Donk, W. A. (1995) *Chem. Biol. 2*, 793−801.
5. Nordlund, P., and Eklund, H. (1995) *Curr. Opin. Struct. Biol. 5*, 758−766.
6. Sjöberg, B. M. (1997) *Struct. Bonding (Berlin) 88*, 139−173.
7. Gräslund A., and Sahlin, M. (1996) *Annu. Rev. Biophys. Biomol. Struct. 25*, 259−286.
8. Stubbe, J., and van der Donk, W. A. (1998) *Chem. Rev. 98*, 705−762.
9. Jordan, A., Pontis, E., Aslund, F., Hellman, U., Gibert, I., and Reichard, P. (1996) *J. Biol. Chem. 271*, 8779−8785.
10. Booker, S., and Stubbe, J. (1993) *Proc. Natl. Acad. Sci. U.S.A. 90*, 8352−8356.
11. Fontecave, M., Eliasson, R., and Reichard, P. (1989) *J. Biol. Chem. 264*, 9164−9170.
12. Sun, X. Y., Harder, J., Krook, M., Jörnvall, H., Sjöberg, B. M., and Reichard, P. (1993) *Proc. Natl. Acad. Sci. U.S.A. 90*, 577−581.
13. Young, P., Andersson, J., Sahlin, M., and Sjöberg, B. M. (1996) *J. Biol. Chem. 271*, 20770−20775.
14. Willing, A., Follmann, H., and Auling, G. (1988) *Eur. J. Biochem. 178*, 603−611.
15. Fieschi, F., Torrents, E., Toulokhonova, L., Jordan, A., Hellman, U., Barbe, J., Gibert, I., Karlsson, M., and Sjöberg, B. M. (1998) *J. Biol. Chem. 273*, 4329−4337.
16. Griepenburg, U., Blasczyk, K., Kappl, R., Hüttermann, J., and Auling, G. (1998) *Biochemistry 37*, 7992−7996.
17. Eliasson, R., Pontis, E., Jordan, A., and Reichard, P. (1996) *J. Biol. Chem. 271*, 26582−26587.
18. Ehrenberg, A., and Reichard, P. (1972) *J. Biol. Chem. 247*, 3485−3488.
19. Nordlund, P., Sjöberg, B. M., and Eklund, H. (1990) *Nature 345*, 593−598.
20. Nordlund, P., and Eklund, H. (1993) *J. Mol. Biol. 232*, 123−164.
21. Uhlin, U., and Eklund, H. (1994) *Nature 370*, 533−539.
22. Kauppi, B., Nielsen, B. B., Ramaswamy, S., Larsen, I. K., Thelander, M., Thelander, L., and Eklund, H. (1996) *J. Mol. Biol. 262*, 706−720.
23. Bollinger, J. M., Tong, W. H., Ravi, N., Huynh, B. H., Edmondson, D. E., and Stubbe, J. (1994) *J. Am. Chem. Soc. 116*, 8015−8023.
24. Sturgeon, B. E., Burdi, D., Chen, S.-X., Huynh, B. H., Edmondson, D. E., Stubbe, J., and Hoffman, B. M. (1996) *J. Am. Chem. Soc. 118*, 7551−7557.
25. Sjöberg, B. M., Reichard, P., Gräslund, A., and Ehrenberg, A. (1978) *J. Biol. Chem. 253*, 6863−6865.
26. Bender, C. J., Sahlin, M., Babcock, G. T., Barry, B. A., Chandrashekar, T. K., Salowe, S. P., Stubbe, J., Lindström, B., Petersson, L., Ehrenberg, A., and Sjöberg, B. M. (1989) *J. Am. Chem. Soc. 111*, 8076−8083.
27. Gerfen, G. J., Bellew, B. F., Un, S., Bollinger, J. M., Stubbe, J., Griffin, R. G., Singel, D. J. (1993) *J. Am. Chem. Soc. 115*, 6420−6421.
28. Hoganson, C. W., Sahlin, M., Sjöberg, B. M., and Babcock, G. T. (1996) *J. Am. Chem. Soc. 118*, 4672−4679.
29. van Dam, P. J., Willems, J.-P., Schmidt, P. P., Pötsch, S., Barra, A.-L., Hagen, W. R., Hoffman, B. M., Andersson, K. K., and Gräslund, A. (1998) *J. Am. Chem. Soc. 120*, 5080−5085.
30. Siegbahn, P. E. M., Blomberg, M. R. A., and Crabtree, R. H. (1997) *Theor. Chim. Acta 97*, 289−300.

31. Rova, U., Goodtzova, K., Ingemarson, R., Behravan, G., Gräslund, A., and Thelander, L. (1995) *Biochemistry 34*, 4267−4275.
32. Mao, S. S., Holler, T. P., Yu, G. X., Bollinger, J. M., Booker, S., Johnston, M. I., and Stubbe, J. (1992) *Biochemistry 31*, 9733−9743.
33. Jordan, A., Gibert, I., and Barbe, J. (1994) *J. Bacteriol. 176*, 3420−3427.
34. Jordan, A., Pontis, E., Atta, M., Krook, M., Gibert, I., Barbe, J., and Reichard, P. (1994) *Proc. Natl. Acad. Sci. U.S.A. 91*, 12892−12896.
35. Jordan, A., Gibert, I., and Barbe, J. (1994) *Gene 167*, 75−79.
36. Eliasson, R., Pontis, E., Jordan, A., and Reichard, P. (1996) *J. Biol. Chem. 271*, 26582−26587.
37. Garriga, X., Eliasson, R., Torrents, E., Jordan, A., Barbe, J., Gibert, I., and Reichard, P. (1996) *Biochem. Biophys. Res. Commun. 229*, 189−192.
38. Allard, P., Barra, A. L., Andersson, K. K., Schmidt, P. P., Atta, M., and Gräslund, A. (1996) *J. Am. Chem. Soc. 118*, 895−896.
39. Babcock, G. T., Barry, B. A., Debus, R. J., Hoganson, C. W., Atamian, M., MacIntosh, L., Sithole, I., and Yocum, C. F. (1989) *Biochemistry 28*, 9558−9565.
40. Tommos, C., Tang, X.-S., Warncke, K., Hoganson, C. W., Styring, S., McCracken, J., Diner, B. A., and Babcock, G. T. (1995) *J. Am. Chem. Soc. 117*, 10325−10335.
41. Un, S., Atta, M., Fontecave, M., and Rutherford, W. (1995) *J. Am. Chem. Soc. 117*, 10713−10719.
42. Un, S., Tang, X.-S., and Diner, B. A. (1996) *Biochemistry 35*, 679−684.
43. Hulsebosch, R. J., van den Brink, J. S., Nieuwenhuis, S. A. M., Gast, P., Raap, J., Lugtenburg, L., and Hoff, A. J. (1997) *J. Am. Chem. Soc. 119*, 8685−8694.
44. Nieuwenhuis, S. A. M., Hulsebosch, R. J., Raap, J., Gast, P., Lugtenburg, J., and Hoff, A. J. (1998) *J. Am. Chem. Soc. 120*, 829−830.
45. Yang, F., Lu, G., and Rubin, H. (1994) *J. Bacteriol. 176*, 6738−6743.
46. Yang, F., Curran, S. C., Li, L.-S. Avarbock, D., Graf, J. D., Chua, M.-M., Lu, G., Salem, J., and Rubin, H. (1997) *J. Bacteriol. 179*, 6408−6415.
47. Cole, S. T., Brosch, R., Parkhill, J., Garnier, T., Churecher, C., Harris, D., Gordon, S. V., Eiglmeier, K., Gas, S., Barry, C. E., Tekaia, F., Badcock, K., Basham, D., Brown, D., Chillingworth, T., Connor, R., Davies, R., Devlin, K., Feltwell, T., Gentles, S., Hamlin, N., Holroyd, S., Hornsby, T., Jagels, K., Krogh, A., McLean, J., Moule, S., Murphy, L., Oliver, K., Osborne, J., Quail, M. A., Rajandream, M.-A., Rogers, J., Rutter, S., Seeger, K., Skelton, J., Squares, R., Squares, S., Sulston, J. E., Taylor, K., Whitehead, S., and Barrell, B. G. (1998) *Nature 393*, 537−544.
48. Fraser, C. M., Gocayne, J. D., White, O., Adams, M. D., Clayton, R. A., Fleischmann, R. D., Bult, C. J., Kerlavage, A. R., Sutton, G., Kelley, J. M., Fritchman, J. L., Weidman, J. F., Small, K. V., Sandusky, M., Fuhrmann, J., Nguyen, D., Utterback, T. R., Saudek, D. M., Phillips, C. A., Merrick, J. M., Tomb, J.-F., Dougherty, B. A., Bott, K. F., Hu, P.-C., Lucier, T. S., Peterson, S. N., Smith, H. O., Hutchison, C. A., and Venter, J. C. (1995) *Science 27*0, 397−403.
49. Åberg, A., Ormö, M., Nordlund, P., and Sjöberg, B. M. (1993) *Biochemistry 32*, 9845−9850.
50. Sjöberg, B. M., Hahne, S., Karlsson, M., Jörnvall, H., Göransson, M., and Uhlin, B. E. (1986) *J. Biol. Chem. 261*, 5658−5662.
51. Barra, A. L., Brunel, L. C., and Robert, J. B. (1990) *Chem. Phys. Lett. 165*, 107−109.
52. Bernhard, W. A., and Fouse, G. W. (1989) *J. Magn. Reson. 82*, 156−162.
53. Schmidt, P. P., Andersson, K. K., Barra, A.-L., Thelander, L., and Gräslund, A. (1996) *J. Biol. Chem. 271*, 23615−23618.
54. Carbett, K., Darnall, D. W., Klotz, I. M., and Williams, R. J. P. (1969) *Arch. Biochem. Biophys. 135*, 419−434.
55. Klabunde, T., Sträter, N., Fröhlich, R., Witzel, H., and Krebs, B. (1996) *J. Mol. Biol. 259*, 737−748.
56. Sahlin, M., Gräslund, A., and Ehrenberg, A. (1986) *J. Magn. Reson. 67*, 135−137.
57. Davydov, A., Schmidt, P. P., and Gräslund, A. (1996) *Biochem. Biophys. Res. Commun. 219*, 213−218.
58. Stone, E. W., and Maki, A. H. (1962) *J. Chem. Phys. 37*, 1326−1333.
59. Sahlin, M., Gräslund, A., Ehrenberg, A., and Sjöberg, B. M. (1982) *J. Biol. Chem. 257*, 366−369.
60. Himo, F., Gräslund, A., and Eriksson, L. A. (1997) *Biophys. J. 72*, 1556−1567.

BI981471P